

# Ovonic Memory Switching in Multimaterial Fibers

Sylvain Danto, Zachary Ruff, Zheng Wang, John D. Joannopoulos, and Yoel Fink\*

We demonstrate the first rewritable memory in thermally drawn fibers. A high tellurium-content chalcogenide glass, contacted by metallic electrodes internal to the fiber structure, is drawn from a macroscopic preform. An externally applied voltage is utilized to switch between a high resistance (OFF) and a low resistance (ON) state; this in turn allows the fibers to function as a memory device reminiscent of the ovonic switch. The difference between the ON and OFF states is found to be four orders of magnitude. The glass–crystal phase transition is localized to micrometer-wide filaments, whose position can be optically controlled along the fiber axis. An architecture that enabled the encoding of multiple bits per fiber is described.

## 1. Introduction

Phase-change materials (PCMs) in the high Te-content system Ge–Sb–Te are widely used in modern data storage media for rewritable optical discs and nonvolatile electronic memory.<sup>[1,2]</sup> PCMs are designed to undergo reversible glass/crystalline phase transitions under optically or electrically induced heating. The phase transition produces a large contrast in the optical or electrical properties, allowing low noise readout. The incorporation of PCMs into flexible fiber-based devices would enable the integration of electrically modulated active systems with unusual properties. Nevertheless, the poor thermomechanical properties of PCMs, particularly their tendency for crystallization and their highly temperature dependent viscosity, make them an unlikely candidate as a fiber material. Hence, to date, attempts to incorporate switching materials in high aspect-ratio devices remain limited to postdrawing coating or encapsulation in yarns of phase-change solid/liquid organic materials, for applications such as smart thermoregulated textiles.<sup>[3]</sup>

Recently, we have developed a fiber processing technique that allows the integration of metal, semiconductor and polymer layers at nanometer feature sizes to perform opto-electronic and acoustic functionalities over meters of active length.<sup>[4–10]</sup>

Dr. S. Danto, Z. Ruff, Dr. Z. Wang, Prof. Y. Fink  
Department of Materials Science and Engineering  
Massachusetts Institute of Technology (MIT)  
Cambridge, MA 02139, USA  
E-mail: yoel@mit.edu

Dr. S. Danto, Z. Ruff, Dr. Z. Wang, Prof. J. D. Joannopoulos, Prof. Y. Fink  
Research Laboratory of Electronics  
MIT, Cambridge, MA 02139, USA  
Prof. Y. Fink  
Institute for Soldier Nanotechnologies  
MIT, Cambridge, MA 02139, USA

DOI: 10.1002/adfm.201002252

Here, for the first time, we present ovonic memory switching in arbitrarily long and flexible multimaterial fibers. Key to this breakthrough is the thermal co-drawing of a high Te-content glass in contact with metallic electrodes. The glass composition is selected for its ability to support a gradually varying temperature–viscosity profile while retaining phase-change behaviors under applied electric fields. Voltage pulses alter the phase of the semiconductor between a high-resistance amorphous (OFF) state and a low-resistance crystalline (ON) state. We first present evidence of an electrically driven phase-change in bulk

materials. Then, we demonstrate ovonic memory switching in fiber devices and the temperature dependence of the threshold voltage. Subsequently, we show that an electro-optical hybrid operation enables the accurate positioning of the filamentary crystallization along the device. Finally, we demonstrate that the fibers have the ability to switch reversibly between the ON and OFF states under current pulses of variable intensity. We envision using this technique to implement multiple independent electronic components along the fiber axis. Other potential applications include the design of crossbar fabric-array flexible electronic devices.

## 2. Results and Discussion

Ovonic memory switching media (named after S. Ovshinsky, who first reported the concept<sup>[11]</sup>) rely on the switching ability of PCMs to store bits of information.<sup>[1,2]</sup> When biased near the threshold voltage ( $V_{th}$ ), amorphous memory-type PCMs spontaneously generate a low-resistance filament, thanks to the filling of charged defect states from injected charged carriers.<sup>[12–14]</sup> Subsequently, the high current through the filament initiates Joule self-heating which causes rapid temperature increase, and ultimately leads to the nucleation and growth of a crystalline phase (SET operation). The resultant crystalline features stabilize the material into a low resistance state even when no voltage is applied. Reversibly, an ON to OFF transition (RESET operation) can occur with the application of an even higher current pulse concentrated along the low-R channel. The current pulse locally melts the crystalline phase which is quenched back into the amorphous state. The difference in the electrical resistances between the two states is typically four orders of magnitude. The development of suitable PCMs for memory switching has mainly progressed with the Te-based eutectic Ge<sub>17</sub>Te<sub>83</sub> alloy doped with elements such as Sb.<sup>[1,2,13]</sup> These compositions exhibit a stable amorphous and crystalline phase and a high phase-change velocity.

Introducing ovonic memory switching to fiber devices requires a tradeoff between the thermal stability of the amorphous semiconductor necessary for the drawing process, and the high instability required in terms of the phase-change. In order to balance these two contradictory requirements, we selected a high Te-content  $\text{Ga}_{10}\text{Ge}_{15}\text{Te}_{75}$  glass (GGT glass) and  $\text{Ge}_{22}\text{As}_{18}\text{Se}_{15}\text{Te}_{45}$  glass (GAST glass). Although the GGT glass exhibits a narrow gap between its glass-transition temperature ( $T_g = 172^\circ\text{C}$ ) and crystallization temperature ( $T_x = 285^\circ\text{C}$ ), it can be drawn down into fibers of tens of metres in length.<sup>[15]</sup> The GAST glass ( $T_g = 188^\circ\text{C}$ ,  $T_x = 332^\circ\text{C}$ ) has been successfully drawn both into IR optical fibers and thermal sensing fibers.<sup>[4,16]</sup> Additionally, both GGT and GAST glasses are chemically similar to  $\text{Ge}_{17}\text{Te}_{83}$  and consequently exhibit favorable switching properties. They both show high tendency for crystallization and high electrical conductivity with a strong temperature dependence. Notably, compositions in the Ga–Ge–Te system ( $\text{Ga}_5\text{Ge}_{19}\text{Te}_{76}$ <sup>[17]</sup>,  $\text{Ga}_{20}\text{Ge}_{30}\text{Te}_{50}$ <sup>[18]</sup>) have been previously investigated for use in phase-change media.

First, we investigated the phase-change conditions of the two selected amorphous semiconductors in the bulk (Figure 1). 1-mm-thick samples were cut from glass rods, polished, and contacted with two electrical probes at the top surface. As the applied bias gradually increases, the current quickly evolves from ohmic to nonlinear behavior (Figure 1a(1)). At the critical voltage  $V_t = 130\text{ V}$ , the OFF to ON transition takes place; the current

dramatically increases and the sample switches to a stable low resistance state. Along with the change, the appearance of a channel connecting the electrodes was observed under an optical microscope (Figure 1a(2)). X-ray micro-diffraction (XRD) analysis confirms the crystalline nature of the conductive channel (Figure 1a(3)). Unlike the OFF state, which is typical of an amorphous material, the XRD pattern of the ON state sample exhibits crystalline peaks, with their indexation matching that of crystalline tellurium. The weak strength of the signal is due to the small fraction of crystallites (filament size:  $\sim 20\ \mu\text{m}$  diameter) compared to the total analyzed volume (X-ray spot size:  $\sim 250\ \mu\text{m}$  diameter). The GAST glass also exhibits memory switching behavior at a higher threshold ( $V_{th} = 700\text{ V}$ ) (Figure 1b(1)). The greater  $V_{th}$  for the GAST glass is consistent with its higher structural stability, lower rate of crystallization, and decreased conductivity ( $\rho_{GGT} = 6.45 \cdot 10^{-5}\ \Omega^{-1}\text{cm}^{-1}$ ,  $\rho_{GAST} = 4.35 \cdot 10^{-7}\ \Omega^{-1}\text{cm}^{-1}$ ). The larger fraction of 3-fold As and 4-fold Ge coordinated atoms in the GAST glass leads to greater crosslinking of the chains of chalcogen elements. The GAST glass also behaves less metallically, because of its lower Te and higher Se content. The filament connecting the electrodes in the ON state is depicted in Figure 1b(2). XRD analysis of the post-switching GAST sample shows a single peak at  $30^\circ$ , suggesting the growth of a field-induced crystalline phase (Figure 1b(3)). The lack of crystallographic information nevertheless prevents unequivocal identification from two possible candidate phases,  $\text{As}_2\text{Ge}_2\text{Te}_5$  or  $\text{GeTe}$ .

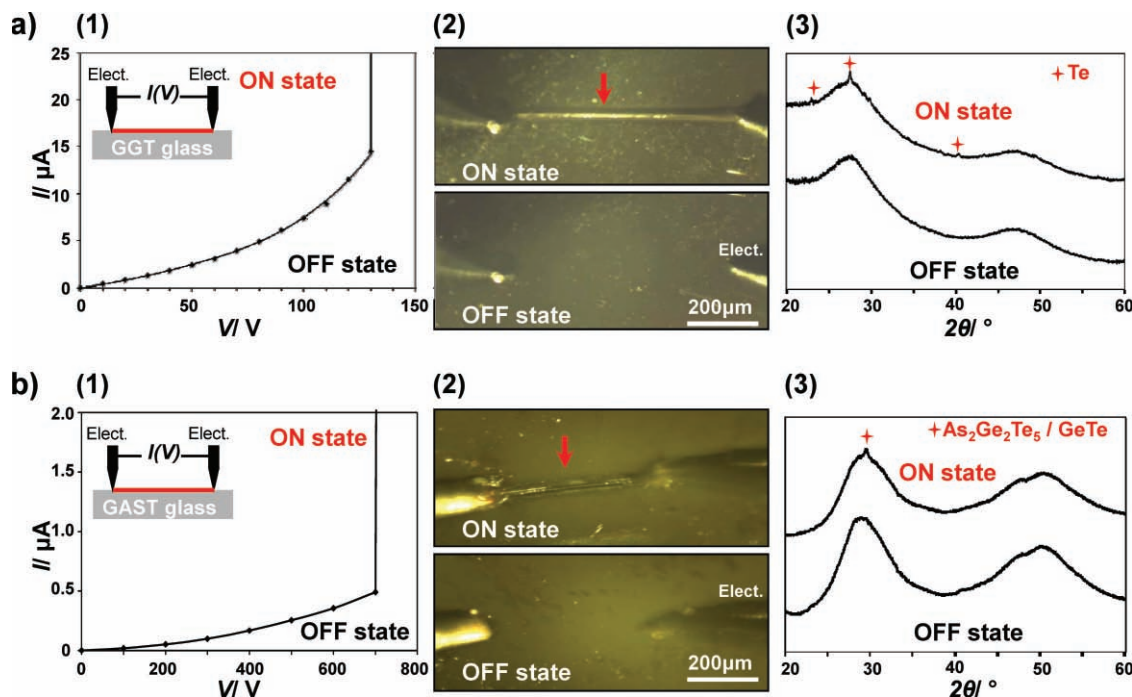


**Figure 1.** Electrically induced crystallization at the surface of bulk glasses ( $\sim 1\text{ mm}$  thick). (a) GGT glass: (1)  $I$ - $V$  characteristic curve; (2) Optical images, bottom shows pre-switching OFF state, top shows post-switching ON state (red arrow: crystalline filament); (3) XRD patterns of an amorphous sample (OFF state) and a sample containing crystalline filaments (ON state, post-switching). Peak indexation confirms the presence of a crystalline phase isostructural to Te. (b) GAST glass: (1)  $I$ - $V$  characteristic curve; (2) Optical images, bottom shows pre-switching OFF state, top shows post-switching ON state (red arrow: crystalline filament); (3) XRD patterns of an amorphous sample (OFF state) and a sample containing crystalline filaments (ON state, post-switching). Peak indexation confirms the presence of a crystalline phase (candidate phases:  $\text{As}_2\text{Ge}_2\text{Te}_5$  or  $\text{GeTe}$ ).

Having established field-induced crystallization in bulk glasses, we now show similar experiments conducted on the cross-section of a GGT fiber device (Figure 2). The fiber is made of a solid-core  $\text{Ga}_{10}\text{Ge}_{15}\text{Te}_{75}$  glass contacted by two  $\text{Zn}_{10}\text{Sn}_{90}$  electrodes ( $T_m = 199^\circ\text{C}$ ) surrounded by a polysulfone (PSU) cladding ( $T_g = 165^\circ\text{C}$ ). A preform is fabricated and then thermally drawn into fibers of tens of meters in length. Afterward, the crosssection of a 1-cm-long sample is carefully polished, as depicted by the scanning electron microscope (SEM) images (Figure 2a). Two probes are used to electrically contact the glass (in order to observe filamentary growth on the cross-section, the probes are *not* put in contact with the Zn–Sn electrodes). Post switching, the SEM image of the fiber reveals a channel connecting the point electrodes (Figure 2b). The OFF to ON transition occurs at  $V_{\text{th}} = 150\text{ V}$ . (Figure 2c). Unlike the OFF state, the XRD pattern of the post switching sample shows a superposition of diffuse halos and small crystallographic peaks (Figure 2d). Their indexation verifies the presence of a semimetallic crystalline phase isostructural to Te and  $\text{Ga}_5\text{Ge}_{19}\text{Te}_{76}$  (additional peaks come from the Zn–Sn electrodes and the resin used to embed the sample).

In the case of standard PCMs, investigations of the switching mechanism show the temperature dependence of the threshold voltage and the electrothermal nature of the breakdown process.<sup>[13,14,19]</sup> We now demonstrate similar results for the aforementioned GGT fiber and in the GAST fiber. The

GAST fiber consists of a solid  $\text{Ge}_{22}\text{As}_{18}\text{Se}_{15}\text{Te}_{45}$  core contacted by four Sn electrodes ( $T_m = 232^\circ\text{C}$ ) and surrounded by a polyethersulfone (PES) cladding ( $T_g = 225^\circ\text{C}$ ) (Figure 3a). For this experiment, 12-cm-long fiber samples are electrically contacted via the Sn electrodes embedded throughout the length of the fibers, and are heated between  $25\text{--}80^\circ\text{C}$  with a hot-plate. Both devices exhibit a clear switching behavior, following a similar temperature dependence (Figure 3b). GGT samples transition to the ON state at lower voltages compared with GAST samples, which agrees with the experiments on the bulk. The exponential temperature dependence of  $V_{\text{th}}$  satisfies the Arrhenius relation:  $V_{\text{th}}(T) = V_0 \exp[\Delta\varepsilon/k_B T]$  where  $\Delta\varepsilon$  is the threshold voltage activation energy,  $V_0$  a constant,  $k_B$  the Boltzmann constant, and  $T$  the absolute temperature (Figure 3c). From the slope of the curves we calculate  $\Delta\varepsilon_{\text{GGT}} = 0.175\text{ eV}$  and  $\Delta\varepsilon_{\text{GAST}} = 0.29\text{ eV}$ . If we now consider the conduction activation energy  $\Delta E_\sigma$  for both glasses ( $\Delta E_\sigma_{\text{GGT}} = 0.30\text{ eV}$ ,<sup>[15]</sup>  $\Delta E_\sigma_{\text{GAST}} = 0.58\text{ eV}$ <sup>[4]</sup>), we obtain  $\Delta\varepsilon/\Delta E_\sigma_{\text{GGT}} = 0.58$  and  $\Delta\varepsilon/\Delta E_\sigma_{\text{GAST}} = 0.5$ . These ratios are in agreement with theory, which predicts that for electrothermal breakdown process, the ratio,  $\Delta\varepsilon/\Delta E_\sigma$  is 0.5.<sup>[19]</sup> Since the resistance of the glasses drops exponentially with the temperature, a positive feedback is established when the bias is above  $V_{\text{th}}$ , fueling the effect of Joule self-heating through increased current at a reduced voltage.

Memory cells typically require a high precision spatial control over localized switching. Here, we demonstrate such spatial control in arbitrarily long fibers using a laser assisted

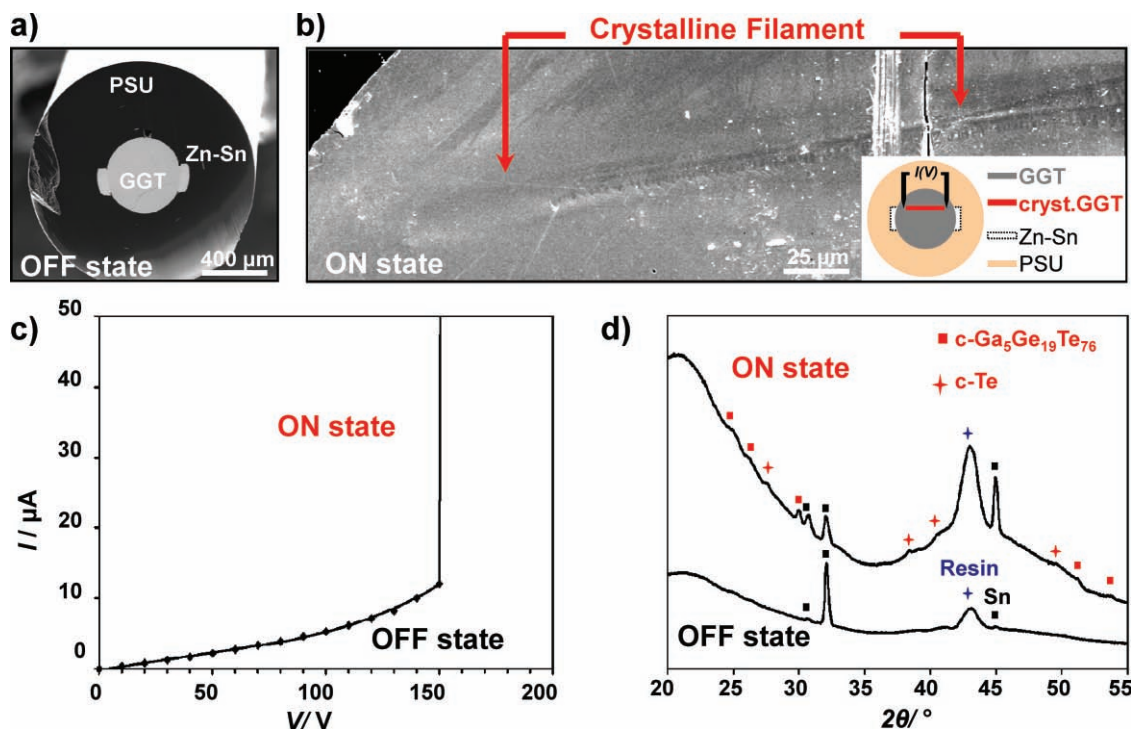


**Figure 2.** Electrically-induced crystallization on the cross-section of a GGT fiber ( $l_{\text{fiber}} = 1\text{ cm}$ ). (a) SEM image of the GGT fiber in the pre-switching OFF state. (b) SEM image of post-switching ON state. (c)  $I$ – $V$  characteristic curve. At the critical value  $V_{\text{th}} = 150\text{ V}$ , the OFF to ON transition takes place. (d) The XRD patterns of an amorphous sample (OFF state) and a sample containing crystalline filaments (ON state, post-switching). Peak indexation confirms the presence of a crystalline phase isostructural to Te and  $\text{Ga}_5\text{Ge}_{19}\text{Te}_{76}$  (supplementary peaks:  $\text{Zn}_{10}\text{Sn}_{90}$  electrodes and resin used to embed the sample).



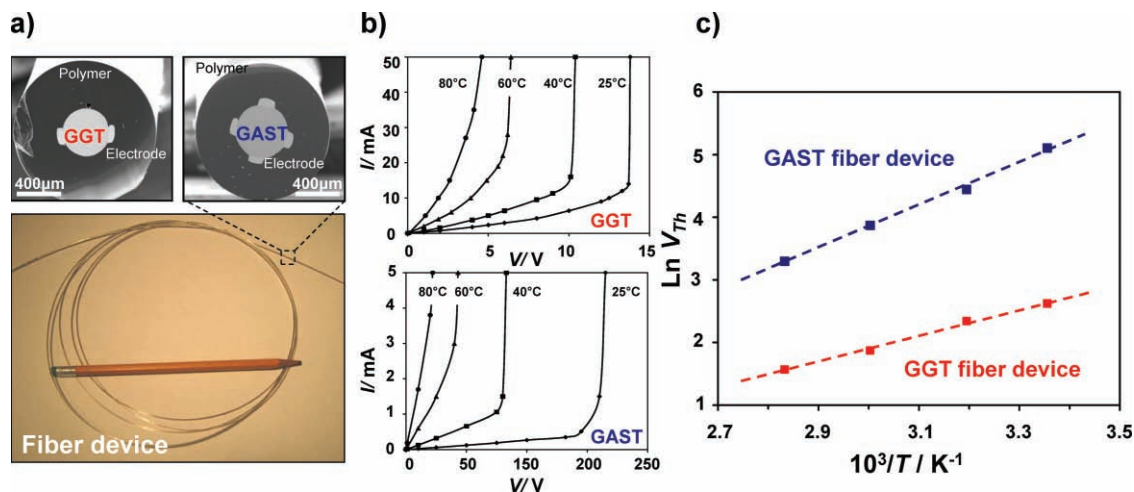


**Figure 3.** Phase-change memory switching in fibers. (a) Photographs of a typical memory fiber (bottom panel). SEM images of the cross-section of a GGT fiber (top left) and a GAST fiber (top right). (b)  $I$ - $V$  characteristics of a GGT fiber (top) and a GAST fiber (bottom) at various temperatures ( $I_{\text{fiber}} = 12$  cm). (c) For both fibers, the threshold voltage as a function of the temperature agrees well with Arrhenius relation (dashed lines).

operation (Figure 4). For comparison, we first locate the crystalline filaments in an electrically switched fiber *without* laser exposure (Figure 4a). A 15-cm-long GAST fiber with adjacent external connections is electrically set to the ON state ( $V_{\text{SET}} = 220$  V,  $R_{\text{ON}} \sim 10^2 \Omega$ ). The resistance is then measured ( $V_{\text{probing}} = 1$  V), while removing sections from the fiber of 1 cm length at a time. Upon removing 7–8 cm of the fiber, the resistance returns to the high value ( $R_{\text{OFF}} \sim 10^6 \Omega$ ). Infrared camera monitoring confirms the electrical measurements (Figure 4a (top)). It shows that, when solely electrically driven, the formation of the highly conductive path occurs at a random site along the device, possibly related to the presence of a defect presence easy generation. By taking advantage of the temperature dependence on  $V_{\text{th}}$ , we next show that we can accurately control the location of the filament by localized laser heating (Figure 4b). A GAST fiber (initial length,  $L = 12$  cm) is placed on an  $x$ - $y$  stage, with the two contacted electrodes facing up. The voltage  $V = 60$  V is applied to bring the current into the nonohmic region, but below the switching threshold. Then we focus an  $\text{Ar}^+$  laser beam ( $P = 20$  mW,  $\lambda = 510$  nm) at  $\sim 0.5$  cm from the end of the fiber, locally heating the glass through the transparent cladding. The laser power is gradually increased and the  $I$ - $V$  response monitored. Upon reaching  $P \sim 120$  mW, the device switches from the OFF<sub>L</sub> state ( $R_{\text{OFF}} \sim 10^6 \Omega$ ) to the ON<sub>L</sub> state ( $R_{\text{ON}} \sim 10^2 \Omega$ ). We then remove the irradiated portion of the fiber by cutting a 1-cm-long section from the end. The resistance of the device subsequently returns to the OFF<sub>L-1</sub> value, nearly identical to the previous OFF<sub>L</sub> value. Therefore, by illuminating the glass, we can locally increase the temperature at a specific site and hence decrease  $V_{\text{th}}$ . In order to show reproducibility in the process, we repeated the same operation seven times with identical results.

Another important feature of PCMs is their ability to cycle reversibly under applied bias between the OFF and ON states. The reversibility is examined in a 12-cm-long GAST fiber (in the case of GGT fiber, no amount of current below the damage threshold of the polymer cladding was able to reset the device

back to the OFF state). The  $I$ - $V$  characteristic SET/RESET cycle follows the schematic pattern described in Figure 5a (inset: SEM crosssection of the GAST fiber). The SET operation consists of raising the voltage above the threshold value ( $V_{\text{th}} \sim 190$  V). As previously discussed, the SET current pulse yields a local increase in the temperature of the glass above its  $T_g$  and the nucleation and growth of a crystalline phase as a result of Joule self-heating. Reversibly, the RESET operation consists of increasing the current until the  $I_{\text{RESET}}$  pulse locally melts the low- $R$  crystalline channel which is then quenched back to the amorphous state. We subjected the device to a complete SET/RESET cycle for two different SET current limitations:  $I_{\text{SET}} = 2.5$  mA and 11.5 mA (Figure 5b). In the case of  $I_{\text{SET}} = 2.5$  mA, the resistance drops by  $\sim 3$  orders of magnitude (a so-called “low-ON state”) and the RESET current is  $I_{\text{RESET}} \sim 4$  mA. In the case of  $I_{\text{SET}} = 11.5$  mA, the resistance fluctuates by  $\sim 4$  orders of magnitude (so-called “High-ON state”) and  $I_{\text{RESET}} \sim 20$  mA. As  $I_{\text{SET}}$  increases from 2.5 to 11.5 mA, the cross-section and thermal stability of the crystalline filament increase. Consequently, the RESET current increases concomitantly with  $I_{\text{SET}}$ , from  $I_{\text{RESET}} = 4$  mA to 20 mA. Following a similar SET/RESET operation over an arbitrary number of 10 cycles, we switch the resistance of a fiber by orders of magnitude.

The fiber-based ovonic memory switching represents the first step towards the implementation of complex circuits into kilometer-long fiber devices. Compared with postdrawing annealing,<sup>[8]</sup> we have significantly improved the crystallization speed of the glass. Combined with the processing of nanofilament arrays,<sup>[7]</sup> we foresee the possibility of using fiber-based resistive switching as an alternative route towards the large scale fabrication of crystalline nanowires. In addition, we anticipate circumventing a major challenge in the breaking of the fiber symmetry along its principle axis. This approach is based, on one hand, on our ability to control the voltage profile along the fiber length, using a high viscosity conductive polymer,<sup>[9]</sup> and, on the other hand, on our control of the phase change localization under laser assisted operation as proposed above. Taking

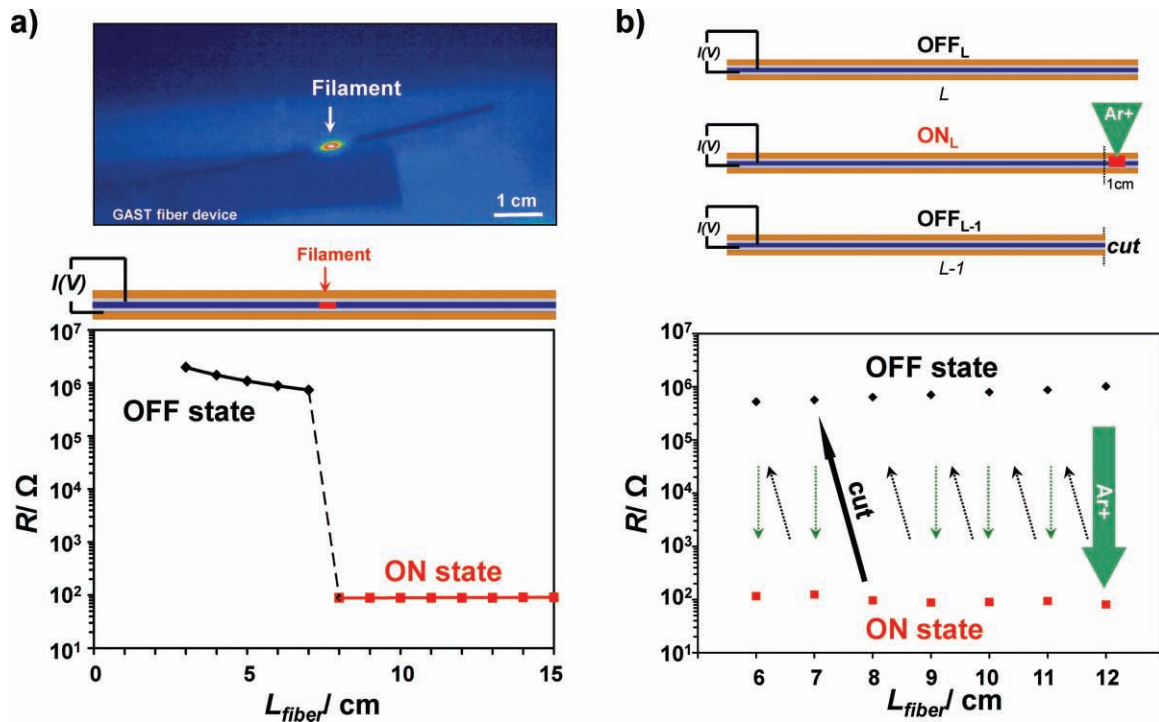


**Figure 4.** Optical positioning of a filament in a GAST fiber. (a) Uncontrolled positioning of the filament. A fiber (initial length: 15 cm) is set to the ON state and the resistance is located using a cut-back method with a 1 cm section removed from the distal end at a time. The fiber reverts to the OFF state when a section of 7–8 cm is removed (top panel: visualization of the local heating from the crystalline filament using an IR camera). (b) Electro-optical positioning of the crystalline filament. A device of length  $L$  (initial length: 12 cm) is biased with a DC voltage of 60 V. An  $\text{Ar}^+$  laser beam ( $\lambda = 510$  nm) illuminates the distal end of the fiber and induces the  $\text{OFF}_L$  to  $\text{ON}_L$  transition. When the irradiated section is removed, the fiber reverts back to the  $\text{OFF}_{L-1}$  state, identical to the  $\text{OFF}_L$  state.

full advantage of these two techniques, we could electrically implement and address multiple yet independent electronic components, such as field effect transistors,<sup>[8]</sup> along one single fiber axis. Beyond one-dimensional single fiber devices, we envision the design of fiber-based fabric-array electronic devices according to a crossbar architecture pattern (Scheme 1).<sup>[20]</sup> In this case, the switching filaments are localized at each

interconnection between an array of fibers and a perpendicular array of metallic wires. As depicted in Scheme 1a, the design of a fiber-based fabric-array memory device would require optimization of the fiber design such as shifting towards a rectangular cross-section to increase surface contact,<sup>[10]</sup> and the use of high-viscosity conductive polycarbonate polymer (c-PC), compatible with thermal drawing, to allow external access to the embedded

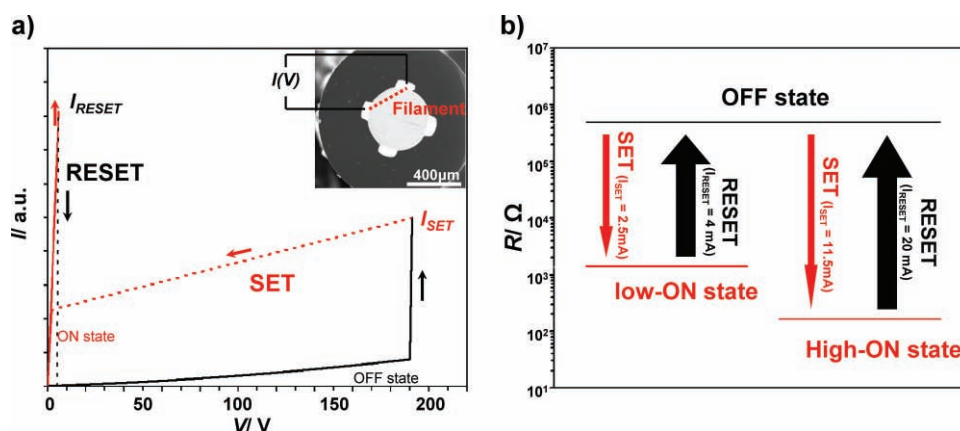
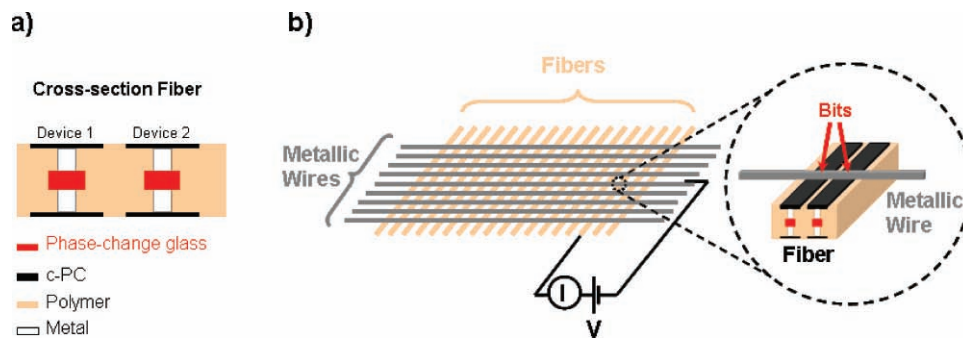


**Figure 5.** Reversible switching in a GAST phase-change memory fiber ( $L_{\text{fiber}} = 12$  cm). (a) The evolution of the current-voltage characteristics in a SET/RESET operation (inset: SEM cross-section GAST fiber). (b) ON/OFF cycling of the device for two different SET conditions ( $I_{\text{SET}} = 2.5$  mA, low-ON state;  $I_{\text{SET}} = 11.5$  mA, high-ON state).



**Scheme 1.** Schematic of a fiber-based fabric-array memory device designed on a crossbar architecture pattern. (a) Cross-section of the fiber (we arbitrarily design a fiber with two devices per cross-section). (b) Multi-bits fiber-based device.

memory devices.<sup>[9]</sup> Moreover, it would also benefit from an increase in the density of memory devices per fiber cross-section to increase the number of “bits” (we arbitrarily show a fiber made of two devices) and the tailoring of the glass composition to lower the phase change power consumption. The thermal drawing of a single perform would allow the fabrication of a multibits fiber-based device, the number of available bits being a direct function of the number of interconnections (Scheme 1b). Multiple levels would be possible as well. These 2D fabric-array devices could be potentially used as RFID (radio frequency identification) tags or sensors.

### 3. Conclusion

In summary, we demonstrate the principle of phase-change switching inside a composite fiber. The codrawing of a high Te-content glass in contact with metallic electrodes enables the electric modulation of the electronic structure of the semiconductor, yielding drastic and reversible variations in the resistance of the device. In addition, we show that an electro-optical hybrid operation enables accurate positioning of the crystalline filament along the fiber axis. The fiber-based ovonic memory switching devices promise new possibilities by bridging two previously unrelated and yet successful application areas for amorphous semiconductors: data storage and fiber optic technologies.

### 4. Experimental Section

**Amorphous Semiconductor Synthesis:** glass rods of composition  $\text{Ga}_{10}\text{Ge}_{15}\text{Te}_{75}$  and  $\text{Ge}_{22}\text{As}_{18}\text{Se}_{15}\text{Te}_{45}$  were prepared from high purity Ge, Ga, As, Se, and Te elements (Alfa Aesar, 5–6N) by the standard melt-quench method. Elements in the appropriate amount were introduced into a quartz ampoule and placed under vacuum ( $\sim 10^{-5}$  Torr). The quartz tube was then sealed and heated in a rocking furnace to 750 °C for 12 h to assure complete homogenization of the melt. The ampoule was quenched in water, annealed at  $\sim T_g$  for 2 h, and cooled to room temperature.

**Preform Preparation and Fiber Drawing:** The  $\text{Ga}_{10}\text{Ge}_{15}\text{Te}_{75}$  fiber device was prepared with  $\text{Sn}_{90}\text{-Zn}_{10}$  electrodes and surrounded by a polysulfone (PSU) cladding. The  $\text{Ge}_{22}\text{As}_{18}\text{Se}_{15}\text{Te}_{45}$  fiber device was prepared with Sn electrodes and surrounded by a polyethersulfone (PES) cladding.

Solid-core fiber device preforms were prepared by sliding a glass rod of 10-mm diameter into a polymer tube having slots cut out. Electrodes were inserted into the slots and additional polymer was wrapped around the metal-semiconductor device until the final preform diameter was  $\sim 27$  mm. The preforms were consolidated under vacuum for  $\sim 30$  minutes (GGT fiber device: 225 °C, GAST fiber device: 260 °C) and then drawn (GGT fiber device:  $\sim 265$  °C, GAST fiber device:  $\sim 290$  °C) in a standard fiber draw tower. With this procedure  $\sim 30$  meters of fiber were drawn with diameters ranging from 0.80 mm to 1.20 mm.

**Bulk Glass and Fiber Device Characterization:** All the characteristic temperatures were measured with a Q1000 TA instruments DSC (heating rate: 10 °C  $\text{min}^{-1}$ ) and were taken to be the onset of the thermal event. X-ray diffraction characterizations were performed with a Bruker D8 Diffractometer (Cu target,  $\lambda = 1.54056$  Å). A selectable collimator, which conditions the X-ray beam to a spot size from 200 to 500  $\mu\text{m}$  diameter, combined with a motorized x–y stage enable microdiffraction. The electrical measurements were performed with a Keithley 6517a electrometer and 6487 picoammeter. Electrical contacts were made to the electrodes by stripping away the cladding and attaching thin wires to the exposed electrodes with conductive Ag paint.

### Acknowledgements

The authors thank S. A. Speakman for technical assistance. This work was supported in part by the MRSEC Program of the US NSF under award number DMR-0819762 and also in part by the US Army Research Office through the ISN at MIT under contract no. W911NF-07-D-0004. We also thank the RLE and CMSE for their support.

Received: October 26, 2010

Published online: February 25, 2011

- [1] S. Raoux, *Annu. Rev. Mater. Res.* **2009**, 39, 25.
- [2] M. Wuttig, N. Yamada, *Nat. Mater.* **2007**, 6, 824.
- [3] S. Mondal, *Appl. Therm. Eng.* **2008**, 28, 1536.
- [4] M. Bayindir, A. F. Abouraddy, J. Arnold, J. D. Joannopoulos, Y. Fink, *Adv. Mater.* **2006**, 18, 845.
- [5] A. F. Abouraddy, M. Bayindir, G. Benoit, S. D. Hart, K. Kuriki, N. D. Orf, O. Shapira, F. Sorin, B. Temelkuran, Y. Fink, *Nat. Mater.* **2007**, 6, 336.
- [6] F. Sorin, O. Shapira, A. F. Abouraddy, M. Spencer, N. D. Orf, J. D. Joannopoulos, Y. Fink, *Nano Lett.* **2009**, 9, 2630.
- [7] D. S. Deng, N. D. Orf, S. Danto, A. F. Abouraddy, Y. Fink, J. D. Joannopoulos, *Appl. Phys. Lett.* **2010**, 96, 023102.

- [8] S. Danto, F. Sorin, N. D. Orf, Z. Weng, S. A. Speakman, J. D. Joannopoulos, Y. Fink, *Adv. Mater.* **2010**, *22*, 4162.
- [9] F. Sorin, G. Lestoquoy, S. Danto, J. D. Joannopoulos, Y. Fink, *Opt. Express* **2010**, *18*, 24264.
- [10] S. Egusa, Z. Wang, N. Chocat, Z. M. Ruff, A. M. Stolyarov, D. Shemuly, F. Sorin, P. T. Rakich, J. D. Joannopoulos, Y. Fink, *Nat. Mater.* **2010**, *9*, 643.
- [11] S. R. Ovshinsky, *Phys. Rev. Lett.* **1968**, *21*, 1450.
- [12] D. Adler, M. S. Shur, M. Silver, S. R. Ovshinsky, *J. Appl. Phys.* **1980**, *51*, 3289.
- [13] D. Adler, S. C. Moss, *J. Vac. Sci. Technol.* **1972**, *9*, 1182.
- [14] D. Adler, *J. Vac. Sci. Technol.* **1973**, *10*, 728.
- [15] S. Danto, P. Houizot, C. Boussard-Pledel, X. H. Zhang, F. Smektala, J. Lucas, *Adv. Funct. Mater.* **2006**, *16*, 1847.
- [16] V. K. Tikhomirov, D. Furniss, A. B. Seddon, J. A. Savage, P. D. Mason, D. A. Orchard, K. L. Lewis, *Infrared Phys. Technol.* **2004**, *45*, 115.
- [17] L. K. Malhotra, Y. Sripathi, G. B. Reddy, *Bull. Mater. Sci.* **1995**, *18*, 725.
- [18] Y. Sripathi, L. K. Malhotra, G. B. Reddy, *Thin Solid Films* **1995**, *270*, 60.
- [19] K. A. Sharaf, *Appl. Phys. A: Mater. Sci. Process.* **1991**, *53*, 218.
- [20] W. Lu, C. Lieber, *Nat. Mater.* **2007**, *6*, 841.